

## THE WFC3 GALACTIC BULGE TREASURY PROGRAM: METALLICITY ESTIMATES FOR THE STELLAR POPULATION AND EXOPLANET HOSTS<sup>1</sup>

THOMAS M. BROWN<sup>2</sup>, KAILASH SAHU<sup>2</sup>, JAY ANDERSON<sup>2</sup>, JASON TURLINSON<sup>2</sup>, JEFF A. VALENTI<sup>2</sup>, ED SMITH<sup>2</sup>, ELIZABETH J. JEFFERY<sup>2</sup>, ALVIO RENZINI<sup>3</sup>, MANUELA ZOCCALI<sup>4</sup>, HENRY C. FERGUSON<sup>2</sup>, DON A. VANDENBERG<sup>5</sup>, HOWARD E. BOND<sup>2</sup>, STEFANO CASERTANO<sup>2</sup>, ELENA VALENTI<sup>7</sup>, DANTE MINNITI<sup>4,6</sup>, MARIO LIVIO<sup>2</sup>, NINO PANAGIA<sup>2,8,9</sup>

*Accepted for publication in The Astrophysical Journal Letters*

### ABSTRACT

We present new UV-to-IR stellar photometry of four low-extinction windows in the Galactic bulge, obtained with the Wide Field Camera 3 on the *Hubble Space Telescope* (*HST*). Using our five bandpasses, we have defined reddening-free photometric indices sensitive to stellar effective temperature and metallicity. We find that the bulge populations resemble those formed via classical dissipative collapse: each field is dominated by an old ( $\sim 10$  Gyr) population exhibiting a wide metallicity range ( $-1.5 \lesssim [\text{Fe}/\text{H}] \lesssim 0.5$ ). We detect a metallicity gradient in the bulge population, with the fraction of stars at super-solar metallicities dropping from 41% to 35% over distances from the Galactic center ranging from 0.3–1.2 kpc. One field includes candidate exoplanet hosts discovered in the SWEEPS *HST* transit survey. Our measurements for 11 of these hosts demonstrate that exoplanets in the distinct bulge environment are preferentially found around high-metallicity stars, as in the solar neighborhood, supporting the view that planets form more readily in metal-rich environments.

*Subject headings:* Galaxy: bulge — Galaxy: formation — Galaxy: stellar content — stars: low-mass — planetary systems — techniques: photometric

### 1. INTRODUCTION

A primary quest of observational astronomy is elucidating the formation history of massive galaxies. This work proceeds on two complementary fronts. High-redshift surveys investigate large galaxy samples over cosmic timescales, but do so with relatively crude age diagnostics and limited spatial information in individual galaxies. Surveys of nearby galaxies investigate a small sample in the present, but can probe discrete structures and obtain diagnostics using photometry of individual stars. The Wide Field Camera 3 (WFC3; MacKenty et al. 2010) on the *Hubble Space Telescope* (*HST*) is a powerful new tool to study galaxy formation in both the high-redshift and local regimes.

We know little about the formation of galaxy bulges, due in part to conflicting evidence regarding our own bulge (see Zoccali 2010). From a populations perspective, our bulge looks like a “classical” bulge – similar to an old, nearly coeval elliptical galaxy. From a morphological perspective, our bulge

looks like a “pseudo-bulge,” with a peanut shape apparently arising from bar-driven secular processes. As summarized by Kormendy & Kennicutt (2004), a range of mechanisms may contribute to bulge formation, with rapid processes in discrete events (e.g., dissipative collapse, mergers of clouds and proto-galaxies) dominating in the early universe, and secular processes (interactions between stars, gas clouds, bars, spiral structure, triaxial halos, etc.) dominating at later times. In broad terms, we see classical bulges if the earlier rapid processes are dominant, and pseudo-bulges if the later slower processes are dominant. However, a new paradigm has recently emerged, driven by observations at  $z \sim 2$ , that reveal the widespread existence of large, rotating, disk galaxies with much higher gas fractions compared to local spirals (Genzel et al. 2008; Förster Schreiber et al. 2009). Such gas-rich, clumpy disks are prone to instabilities that can lead to bulge formation at early cosmic epochs and over timescales much shorter than those traditionally associated with secular instabilities in local spirals (e.g., Immeli et al. 2004; Elmegreen et al. 2009). These processes should imprint distinct age and metallicity gradients upon the bulge stellar populations. For example, bulge evolution dominated by secular processes (such as bar instabilities) is not expected to produce radial metallicity gradients, but is expected to produce younger stars in the bulge outskirts (see Zoccali 2010 and references therein).

To shed light on these processes, our WFC3 Galactic Bulge Treasury program uses the new panchromatic capabilities of *HST* to probe the bulge stellar populations as a function of position (Brown et al. 2009). One of these bulge fields includes 13 candidate exoplanet hosts discovered via the SWEEPS transit survey (Sahu et al. 2006), and so our photometry can also demonstrate where these hosts fall within the bulge metallicity distribution function (MDF). Because WFC3 is a relatively new addition to *HST*, the full analysis of these data will require improvements in the calibration pipeline, data reduction, and analysis techniques, but we present here a look at preliminary results from our program.

<sup>1</sup> Based on observations made with the NASA/ESA *Hubble Space Telescope*, obtained at STScI, which is operated by AURA, Inc., under NASA contract NAS 5-26555.

<sup>2</sup> Space Telescope Science Institute, 3700 San Martin Drive, Baltimore, MD 21218; thrown@stsci.edu, ksahu@stsci.edu, jayander@stsci.edu, tumlinson@stsci.edu, valenti@stsci.edu, edsmith@stsci.edu, jeffery@stsci.edu, ferguson@stsci.edu, bond@stsci.edu, stefano@stsci.edu, mlivio@stsci.edu, panagia@stsci.edu

<sup>3</sup> Osservatorio Astronomico, Vicolo Dell’Osservatorio 5, I-35122 Padova, Italy; alvio.renzini@oapd.inaf.it

<sup>4</sup> P. Universidad Católica de Chile, Departamento de Astronomía y Astrofísica, Casilla 306, Santiago 22, Chile; mzoccali@astro.puc.cl, dante@astro.puc.cl

<sup>5</sup> Department of Physics and Astronomy, University of Victoria, P.O. Box 3055, Victoria, BC, V8W 3P6, Canada; vandenbe@uvic.ca

<sup>6</sup> Vatican Observatory, V-00120 Vatican City State, Italy

<sup>7</sup> European Southern Observatory, Karl Schwarzschild-Straße 2, D-85748 Garching bei München, Germany; valenti@eso.org

<sup>8</sup> INAF-CT, Osservatorio Astrofisico di Catania, Via S. Sofia 78, I-95123 Catania, Italy

<sup>9</sup> Supernova Limited, OYV #131, Northsound Road, Virgin Gorda, British Virgin Islands.

**Table 1**  
Bulge Fields

Name	$l$ (deg)	$b$ (deg)	$R_{min}^a$ (kpc)	$A_V$ (mag)	$A_V$ Reference
Stanek’s Window	+0.25	-2.15	0.32	2.6	Stanek (1998)
SWEEPS <sup>b</sup>	+1.26	-2.65	0.43	2.0	Sahu et al. (2006)
Baade’s Window	+1.06	-3.81	0.58	1.6	Baade (1963)
OGLE29 <sup>c</sup>	-6.75	-4.72	1.21	1.5	Sumi (2004)

<sup>a</sup>Projected Galactocentric distance, assuming a distance of 8.4 kpc (Reid et al. 2009).

<sup>b</sup>Sagittarius Window Eclipsing Extrasolar Planet Survey

<sup>c</sup>Optical Gravitational Lensing Experiment

## 2. OBSERVATIONS AND DATA REDUCTION

Our program is summarized in Brown et al. (2009), but we give a brief summary here. We obtained deep photometry in four low-extinction bulge windows (Table 1) with *HST*/WFC3. To measure proper motions, we will repeat observations in three fields, while the fourth (SWEEPS) was observed previously with *HST* by Sahu et al. (2006). WFC3 has two imaging channels: a UVIS channel comprised of two  $4k \times 2k$  UV/optical CCDs, and an IR channel employing a single  $1k \times 1k$  HgCdTe array. We observed these bulge fields with five channel/filter combinations: UVIS/F390W (hereafter  $C$ ; exposure time 11180 s), UVIS/F555W ( $V$ ; 2283 s), UVIS/F814W ( $I$ ; 2143 s), IR/F110W ( $J$ ; 1255 s), and IR/F160W ( $H$ ; 1638 s). The bulge images were dithered to allow  $2 \times 2$  resampling of the point spread function (PSF); because the IR channel has a smaller field of view ( $123 \times 136''$ ) than the UVIS channel ( $162 \times 162''$ ), additional offsets provided IR coverage of the full UVIS image area. As part of this program, we also observed six star clusters in the same filters, although with less exposure time and little dithering; the resulting color-magnitude diagrams (CMDs) are much noisier than the bulge CMDs, but sufficient to determine ridge lines and calibrate isochrone transformations. The first epoch of observations spans 2009 Oct to 2010 Sep.

The pipeline currently applies a mix of calibrations from ground and preliminary in-flight measurements. We registered, geometrically corrected, and combined the calibrated images using DRIZZLE (Fruchter & Hook 2002), with rejection of hot pixels and cosmic rays for the UVIS images (cosmic rays are removed during the pipeline processing of the non-destructive IR readouts). Using DAOPHOT-II (Stetson 1987), we performed PSF-fitting photometry in the UVIS images and aperture photometry (with neighboring PSFs subtracted) in the IR images. The photometry was corrected to the Vegamag zeropoints of Kalirai et al. (2009a, 2009b), using relatively isolated stars. CMDs for the main-sequence (MS) population in each field are shown in Figure 1.

It is worth noting some limitations of the current reduction. The flat-field corrections are based upon ground tests, with residual spatial variations in sensitivity at the  $\sim 5\%$  level. The geometric distortion correction is undergoing significant revisions, limiting image registration accuracy. The photometric zeropoints were calculated with a subset of the in-flight calibration standards. Some of the UVIS exposure times are short, to provide giant star photometry in each field, but with photometric accuracy currently limited by uncertainties in the CCD charge transfer efficiency. The IR detectors exhibit persistence, elevating the dark current where a bright source has recently illuminated the detector; a future persistence correc-

tion will reduce the photometric noise for the faint stars.

## 3. ANALYSIS

### 3.1. Population Age

The IR CMD of low-mass MS stars exhibits a “knee” at  $\sim 0.5 M_{\odot}$ , due to collisionally-induced  $H_2$  absorption, which serves as a standard candle (Bono et al. 2010). Our IR photometry reaches stars well below this knee (Figure 1). The magnitude difference between the knee and the MS turnoff (MSTO) is approximately constant across our fields, indicating a predominantly old ( $\sim 10$  Gyr) population in each field. The characterization of any subtle variations in the age distribution with position in the bulge will require further analysis.

### 3.2. Anomalous Extinction

As demonstrated by Brown et al. (2009), our five photometric bands can be combined to provide reddening-free indices of temperature [ $t$ ] and metallicity [ $m$ ] in the stellar population. Specifically, for a given extinction law (parameterized by  $R_V \equiv A_V/E(B-V)$ ), the  $[Fe/H]$  inferred from these indices varies by only  $\sim 0.1$  dex when  $A_V$  varies by a magnitude (see Figures 3 and 4 of Brown et al. 2009). For old MS stars reddened with a Galactic average extinction law (Fitzpatrick 1999;  $R_V = 3.1$ ), these indices can be defined as:

$$[t] \equiv (V-J) - 5.8 \times (J-H) \quad (1)$$

and

$$[m] \equiv (C-V) - 0.90 \times (V-I). \quad (2)$$

However, significant deviations from the Galactic average extinction law will shift the distribution in the [ $m$ ] vs. [ $t$ ] plane, because the coefficients in these indices depend upon the reddening vectors in each color. Such shifts are expected here, because Sumi (2004) has found significant variations in  $R_I \equiv A_V/E(V-I)$  toward Galactic bulge fields. The large coefficient (5.8) in the [ $t$ ] index makes it particularly sensitive to random and systematic errors in  $J-H$ . To facilitate the comparison of the populations in each field, we applied a correction for this variation in extinction law before calculating the [ $m$ ] and [ $t$ ] indices. We derived these color shifts by comparing the MS loci of the bulge populations in CMDs of  $C$  vs.  $C-V$ ,  $V$  vs.  $V-I$ ,  $I$  vs.  $I-J$ , and  $J$  vs.  $J-H$ . Although the color distribution within the MS locus varies from field to field, the characteristic shape and boundaries of the MS locus in each field exhibit little variation, such that our shifts allow the loci to be aligned in color to an accuracy of  $\sim 0.01$  mag. To this end, we aligned the MS locus in each field to that in Baade’s Window. The implied extinction curve, when compared to the Galactic average ( $R_V = 3.1$ ) with both normalized at the red end ( $H$ ), differs by less than 0.1 mag in any band, and by less than 0.02 mag if  $2.8 < R_V < 3.1$ . Note that our extinction law corrections are completely empirical; they are consistent with a somewhat lower  $R_V$  at decreasing distance from the Galactic center, but do not allow us to derive the actual value of  $R_V$  at an interesting level of confidence. We assume that the extinction law varies little within the relatively small *HST* field of view.

### 3.3. Metallicity Distributions in the Bulge Populations

Once the variation in extinction law is corrected (see §3.2), we can compare the MDFs in each field. To restrict the analysis to a relatively narrow temperature range where the indices are well-behaved, we selected stars between the MSTO and a

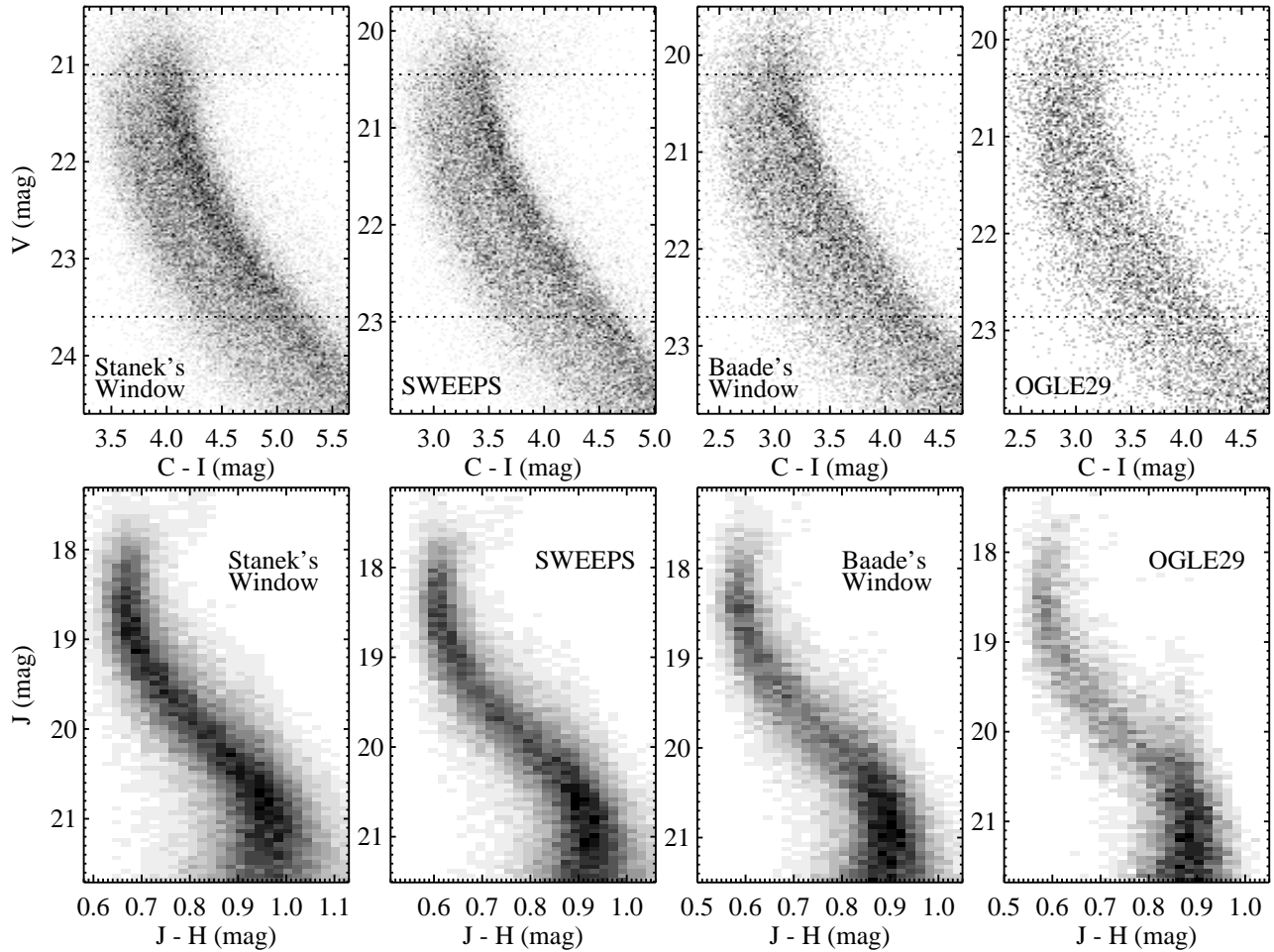


**Figure 1.** CMDs (grey shading) for our bulge fields, binned into Hess diagrams with a linear stretch. The dashed lines in the top panels isolate stars on the upper 2.5 mag of the MS. In the inner fields (Stanek’s Window and SWEEPS), the  $C-I$  color distribution on the MS is bimodal, with a strong red ridge and a fainter blue ridge. Our metallicity index indicates that the red ridge arises from the large number of metal-rich stars, while the blue ridge is due to color degeneracy at low metallicity. CMDs constructed from bands at wavelengths longer than  $C$  (e.g.,  $V$  and  $I$  in Sahu et al. 2006) do not show this bimodality because they are much less sensitive to metallicity.

point 2.5 mag fainter in  $V$  (Figure 1; dashed lines). These relatively bright stars are also well above the detection limits in each field, with small photometric errors due to photon counts and stellar crowding.

The distributions in the  $[m]$  vs.  $[t]$  plane for each field are shown in Figure 2. For comparison, we show the expectations from a set of 10 Gyr isochrones spanning a wide range in  $[\text{Fe}/\text{H}]$  (VandenBerg et al. 2006), transformed into the  $[m]$  vs.  $[t]$  plane using the NextGen grid of synthetic spectra (Hauschildt et al. 1999; updated). We note that new evolutionary tracks and isochrones, accounting for helium diffusion and recent advances in basic stellar physics, are being computed for application to these data (by D.A.V.). As with the photometry, the isochrones are shown from the MSTO to a point 2.5 mag fainter in  $V$ . Spectroscopy of the bulge population indicates significant enhancement in  $[\alpha/\text{Fe}]$  at low metallicity, trending to less enhancement as one approaches  $[\text{Fe}/\text{H}] = 0$  (Lecureur et al. 2007). To mimic that trend, our chosen isochrones assume  $[\alpha/\text{Fe}] = 0.3$  for  $[\text{Fe}/\text{H}] \leq 0$  and  $[\alpha/\text{Fe}] = 0.0$  for  $[\text{Fe}/\text{H}] = 0.5$ . The synthetic spectra assume the same  $\alpha$ -enhancement, but are interpolated from spectra with  $[\alpha/\text{Fe}]$  values of 0, 0.2, and 0.4. Loci of constant metallicity form approximately parallel lines in the diagram, with  $[m] = [m_0] - 0.6 \times [t]$ , such that interpolation between these lines provides a metallicity estimate for each star. The derived

MDFs are shown in Figure 2 (histogram insets). In Baade’s Window, our MDF at  $[\text{Fe}/\text{H}] > -0.5$  is similar to that of Zoccali et al. (2008; from spectroscopy of giants) but has more stars at lower metallicities.

The inner fields (Stanek’s Window and SWEEPS) exhibit a distinctly bimodal distribution of color in the  $V$  vs.  $C-I$  CMDs (Figure 1), while the outer fields (Baade’s Window and OGLE29) exhibit a bimodal distribution in the  $[m]$  vs.  $[t]$  plane (Figure 2), which is reflected in the inferred MDFs. This is due to the nonlinear relationship between the indices, traditional CMD colors, and chemical composition. If the position in the  $[m]$  vs.  $[t]$  plane is taken as an indication of metallicity, the stars at  $[\text{Fe}/\text{H}] > 0$  overwhelmingly lie in the prominent red ridge of the  $V$  vs.  $C-I$  CMDs, while the stars at  $[\text{Fe}/\text{H}] < -1$  tend to lie in the weaker blue ridge of these CMDs.

Brown et al. (2008) discussed the advantages of the  $[m]$  vs.  $[t]$  diagram regarding depth effects, but made no mention of binaries. In a CMD, depth blurs the photometric distribution along the ordinate, blurring the inferred MDF when comparing to isochrones, but a color-color diagram is insensitive to depth. In a CMD, binaries are brighter and redder than the single-star sequence; comparison of binaries to isochrones can thus overestimate their metallicities. In our color-color diagram, a companion of either equal or much lower mass will not shift the position of the primary, but a companion

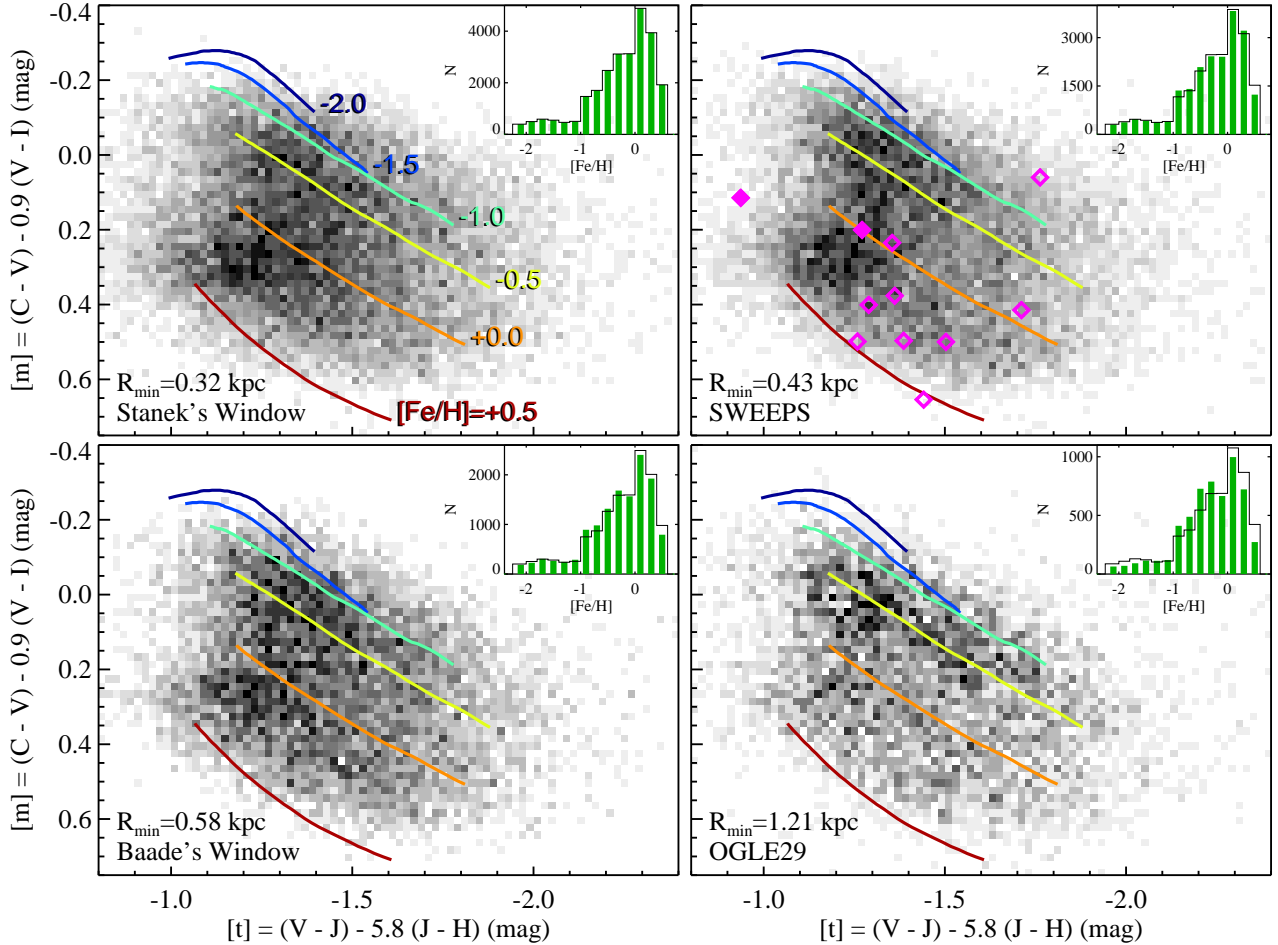


**Figure 2.** Broad-band indices of temperature and metallicity for stars on the upper 2.5 mag of the MS in each bulge field (*grey shading*). For a given extinction law, these indices are insensitive to the amount of reddening, but the photometry here has been corrected for field-to-field variations in reddening law (see §3.2). The curves represent the upper MS in 10 Gyr isochrones, ranging in  $[\text{Fe}/\text{H}]$  from  $-2.0$  to  $+0.5$  (*labeled*). In the SWEEPS field, candidate exoplanet hosts are indicated (Sahu et al. 2006; *diamonds*), clustering at high metallicity. Radial velocities support the planetary nature of two exoplanet candidates (*filled diamonds*). The inset for each panel shows the estimated MDF in each field (*green bars*), along with that in Stanek’s Window for comparison (*black histogram*; normalized to the counts in each field). Note that the metallicity estimates are degenerate at low metallicity, artificially producing a long metal-poor tail in the MDF. The general tendency is for decreasing metallicity at increasing distance from the Galactic center.

that is only somewhat fainter and cooler will artificially shift the implied metallicity lower (i.e., opposite to the CMD effect). This is because the secondary has a larger impact on  $[t]$  than  $[m]$ . The metallicities of any binaries in our field can be underestimated by up to  $\sim 0.3$  dex.

From a strictly statistical perspective, a Kolmogorov-Smirnov (KS) test indicates that no pair of these fields has populations drawn from the same distribution; the chance is 3% for the populations in the SWEEPS field and Baade’s Window, and  $\ll 1\%$  for any other pair. The MDFs in the two innermost fields (Stanek’s Window and SWEEPS) are similar in appearance, although the metallicity appears to be shifted to slightly lower  $[\text{Fe}/\text{H}]$  in the SWEEPS field. Progressing outward, Baade’s Window and the OGLE29 field each exhibit more stars shifting to lower metallicities, with the MDFs appearing more bimodal than that in the interior fields, due to a stronger presence of relatively metal-poor stars. Taking the relationship between indices and  $[\text{Fe}/\text{H}]$  at face value, the fraction of stars with super-solar metallicities drops as one progresses outward through the fields: Stanek’s Window (41%), SWEEPS (39%), Baade’s Window (38%), and OGLE29 (35%). Rich et al. (2007) found no gradient in the bulge metallicity when comparing the spectroscopic metal-

licities of 17 M giants in the inner bulge to 14 M giants in Baade’s window, but given their small sample, their result may be consistent with our findings. Zoccali et al. (2008) found the bulge to decrease in metallicity along the minor axis beyond  $4^\circ$ .

Note that our measured MDF variation is for the general population in each field, and cannot be investigated for the bulge in isolation without proper-motion cleaning of the foreground stars. We have used the TRILEGAL Galaxy model, with its default parameters (Girardi et al. 2005), to estimate that the foreground thin disk, thick disk, and halo together contribute 5–9% of the total population in each field, with higher contamination at increasing distance from the Galactic center. We performed a preliminary proper-motion cleaning of the catalog in the SWEEPS field, by comparing our astrometry to that in Sahu et al. (2006), and assuming the relative disk and bulge velocities of Clarkson et al. (2008). This cleaning clearly reduces the presence of CMD features associated with the disk foreground (e.g., the blue plume above the old MSTO), but the MDF in the remaining bulge population is not significantly changed from that shown in Figure 2.

The combination of isochrones and synthetic spectra employed in Figure 2 was chosen because it spans nearly the

full range of photometric indices in each field, demonstrating the nonlinear relationship between indices and  $[\text{Fe}/\text{H}]$ . However, the zeropoint of the  $[\text{Fe}/\text{H}]$  scale is uncertain at the level of 0.2–0.3 dex, depending upon the actual extinction law in Baade’s Window (changing  $R_V$  by 0.1 shifts the implied  $[\text{Fe}/\text{H}]$  by 0.1 dex), the assumed abundance pattern (e.g.,  $[\alpha/\text{Fe}]$  as a function of  $[\text{Fe}/\text{H}]$ , particularly at high  $[\text{Fe}/\text{H}]$ ), the photometric zeropoints, and the spectral library employed in the isochrone transformation. Putting the empirical ridge lines of our star clusters (§2) in the same  $[m]$  vs.  $[t]$  plane would imply our assumed  $[\text{Fe}/\text{H}]$  scale underestimates the true  $[\text{Fe}/\text{H}]$  by  $\sim 0.2$ –0.3 dex down to  $[\text{Fe}/\text{H}] \approx -1.5$ , and that our metallicity scale is degenerate at lower metallicities. The offset may be a real systematic error in our metallicity scale, but it may also be due to distinctions in the reddening law and/or abundance pattern between the cluster and bulge populations. The cluster photometry was not corrected for variations in extinction law in the same manner used for the bulge fields, because the MS locus for each cluster is very distinct from that in the bulge, given the single metallicity yet noisier photometry.

### 3.4. Metallicities of the Candidate Exoplanet Hosts

Our SWEEPS field includes 13 of the 16 candidate exoplanet hosts found in the *HST* transit survey of Sahu et al. (2006). Two of these 13 candidates are too faint and red to appear in our *C* images, but the remaining 11 have photometry enabling their placement in the  $[m]$  vs.  $[t]$  plane for the general SWEEPS population (Figure 2; *diamonds*). Two of these 11 candidates have radial velocities that support their planetary nature, and are highlighted in Figure 2 (*filled diamonds*). Although the zeropoint for our assumed  $[\text{Fe}/\text{H}]$  scale is uncertain at the level of  $\sim 0.2$ –0.3 dex (see §3.3), the relative  $[\text{Fe}/\text{H}]$  measurements for the exoplanet hosts and the general population in the SWEEPS field are much more secure, because the same systematic uncertainties apply to both. It is clear from Figure 2 that the candidate exoplanet hosts predominantly fall in the metal-rich end of the bulge MDF – a population that is already skewed toward high metallicity. Aside from a single candidate at the metal-poor end of the distribution, the remaining 10 candidates are more metal-rich than half the population, with 7 in the top quartile. A KS test of the implied metallicities in the exoplanet hosts and general population indicates that the chance they are both drawn from the same parent population is less than 2%.

## 4. DISCUSSION

We have performed a preliminary analysis of the data from our WFC3 Galactic Bulge Treasury Program. Keeping in mind the various systematic uncertainties at this stage, our analysis of the dwarf stars supports the picture of the bulge gleaned from investigations of the brighter giant stars (see Zoccali 2010 and references therein). Our IR photometry reaches the knee on the lower MS, and indicates that the population is predominantly old ( $\sim 10$  Gyr) in all of the bulge fields, with no obvious age gradient. The declining metallicities at increasing radius are seemingly inconsistent with the secular processes that are traditionally associated with the formation of a peanut-shaped bulge. Our findings are consistent with a classical bulge formed via rapid dissipative collapse (either monolithic or via the merger of independent components), but also consistent with a recently emerging formation paradigm, motivated by observations of gas-rich spirals at  $z \sim 2$  (Genzel et al. 2008; Förster Schreiber et al. 2009). In this new paradigm, instabilities in gas-rich disks can drive early bulge formation over rapid timescales (e.g., Immeli et al. 2004; Elmegreen et al. 2009).

Of the hundreds of extrasolar planets discovered to date, most have been found in the solar neighborhood via radial-velocity measurements. A notable exception is the discovery of 16 candidate exoplanet hosts in the SWEEPS transit survey of the Galactic bulge (Sahu et al. 2006). Our multi-band photometry of 11 of these hosts demonstrates that they fall almost exclusively at the high end of the MDF in this high-density, metal-rich field. Exoplanets in the distinct environment of the solar neighborhood are also found preferentially at high metallicity (e.g., Fischer & Valenti 2005). Out of the  $\sim 500$  exoplanets discovered to date whose orbital periods range from a fraction of a day to well over five years,  $> 100$  have orbital periods less than five days, implying significant migration since formation. The correlation of such planets with stars of high metallicity probably indicates that planets are preferentially formed in high-metallicity environments, or alternatively that planets migrate more easily under such conditions.

Support for Program 11664 was provided by NASA through a grant from STScI, which is operated by AURA, Inc., under NASA contract NAS 5-26555. MZ acknowledges Fondecyt Regular 1085278. AR acknowledges ASI for support via the grant “COFIS-Analisi Dati.” We appreciate useful discussions with J. Kalirai and A. Dotter.

## REFERENCES

- Baade, W. 1963, *Evolution of Stars and Galaxies* (Cambridge: Harvard Univ. Press), 277
- Bono, G., et al. 2010, *ApJ*, 708, L74
- Brown, T.M., et al. 2009, *AJ*, 137, 3172
- Clarkson, W., et al. 2008, *ApJ*, 684, 1110
- Elmegreen, B.G., Elmegreen, D.M., Fernandez, M.X., & Lemonias, J.J. 2009, *ApJ*, 692, 12
- Fitzpatrick, E.L. 1999, *PASP*, 111, 63
- Fischer, D.A., & Valenti, J. 2005, *ApJ*, 622, 1102
- Förster Schreiber, N.M., et al. 2009, *ApJ*, 706, 1364
- Fruchter, A.S., & Hook, R.N. 2002, *PASP*, 114, 144
- Girardi, L., Groenewegen, M.A.T., Hatziminaoglou, E., & da Costa, L. 2005, *A&A*, 436, 895.
- Genzel, R., et al. 2008, *ApJ*, 687, 59
- Hauschildt, P.H., Allard, F., & Baron, E. 1999, *ApJ*, 512, 377
- Immeli, A., Samland, M., Gerhard, O., & Westera, P. 2004, *A&A*, 413, 547
- Kalirai, J.S., et al. 2009a, in *Instrum. Sci. Rep. WFC3 2009-30*
- Kalirai, J.S., et al. 2009b, in *Instrum. Sci. Rep. WFC3 2009-31*
- Kormendy, J., & Kennicutt, R.C. 2004, *ARA&A*, 42, 603
- Lecureur, A., et al. 2007, *A&A*, 465, 799
- MacKenty, J.W., Kimble, R.A., O’Connell, R.W., Townsend, J.A. 2010, *SPIE*, 7731, 27
- Reid, M.J., et al. 2009, *ApJ*, 700, 137
- Rich, R.M., Origlia, L., & Valenti, E. 2007, *ApJ*, 665, L119
- Sahu, K., et al. 2006, *Nature*, 443, 534
- Stanek, K.Z. 1998, *ApJL*, submitted, astro-ph/9802307
- Stetson, P. 1987, *PASP*, 99, 191
- Sumi, T. 2004, *MNRAS*, 349, 193
- VandenBerg, D.A., Bergbusch, P.A., & Dowler, P.D. 2006, *ApJS*, 162, 375
- Zoccali, M. 2010, in *IAU Symp. 265, Connecting First Stars to Planets, ed. K. Cunha, M. Spite, & B. Barbuy* (Cambridge: Cambridge Univ. Press), 271
- Zoccali, M., et al. 2008, *A&A*, 486, 177